SCIENCE CHINA
Information Sciences

• RESEARCH PAPER •

June 2026, Vol. 69, Iss. 6, 162407:1–162407:7
https://doi.org/10.1007/s11432-025-4761-5

Optical-chaos temporal ghost imaging

Rong ZHANG[1,2], Anbang WANG[2,3*], Longsheng WANG[1], Zhiwei JIA[1], Yuncai WANG[2,3] & Yuwen QIN[2,3]

[1]*Key Laboratory of Advanced Transducers and Intelligent Control System, Ministry of Education, College of Physics and Optoelectronics, Taiyuan University of Technology, Taiyuan 030024, China*
[2]*Key Laboratory of Photonic Technology for Integrated Sensing and Communication, Ministry of Education, Guangdong University of Technology, Guangzhou 510006, China*
[3]*Guangdong Provincial Key Laboratory of Information Photonics Technology, Institute of Advanced Photonics Technology, School of Information Engineering, Guangdong University of Technology, Guangzhou 510006, China*

Received 8 October 2025/Revised 8 December 2025/Accepted 15 January 2026/Published online 8 May 2026

Abstract Temporal ghost imaging (TGI) enables high-speed information reconstruction from low-bandwidth detection by leveraging self-correlation properties of random light signals. Here, we experimentally demonstrate for the first time the chaos-based TGI using an optical-feedback semiconductor laser. Results reveal the effects of feedback strength and time delay signature and find that the low-frequency energy of chaotic signal within the slow-detection bandwidth determines the imaging quality. By optimizing feedback strength, TGI with a quality factor beyond 3 for 8-Gbit/s NRZ signals is achieved by using a chaotic laser with a relaxation frequency of 6 GHz and 1-GHz detection bandwidth. This work introduces a promising TGI technique, because the use of chaotic lasers overcomes the limitations of conventional random sources in signal amplitude and system integration. Furthermore, considering the phenomenon of chaotic synchronization, this work has the potential to inspire research on secure information transmission based on chaos TGI.

Keywords temporal ghost imaging, correlated imaging, optical chaos, chaotic laser, semiconductor lasers, fast information reconstruction

Citation Zhang R, Wang A B, Wang L S, et al. Optical-chaos temporal ghost imaging. Sci China Inf Sci, 2026, 69(6): 162407, https://doi.org/10.1007/s11432-025-4761-5

1 Introduction

Ghost imaging is an advanced correlated imaging technique initially demonstrated with quantum-entangled photon pairs and later extended to classical domains [1–4]. Inspired by spatial ghost imaging, temporal ghost imaging (TGI) introduces a novel approach for temporal domain measurement, which enables reconstruction of high-speed temporal objects from low-bandwidth detection [5–9]. This unique capability leverages slow detectors that significantly reduce system cost and complexity while ensuring compatibility with bandwidth-limited scenarios [10–12]. Generally, this compressive imaging technology uses a random light measured by a fast detector as a reference, and another replicated light that interacts with the temporal object is measured by a slow detector as a test signal. The object is then reconstructed by correlating these two signals. Neither signal alone suffices for recovery, and TGI further demonstrates a significant anti-interference capability. Therefore, TGI has attracted extensive attention since the first experimental demonstration reported by Ryczkowski et al. [6]. It has promising applications in high-speed data transmission [13–20], ultrafast sensing [21–23], and device response detection [24–26] through random light sources or random digital signals. The TGI has also been extended from light waves to X-rays and microwave bands [17, 18, 20, 21, 23, 27–30].

The optical sources for TGI should have random intensity fluctuations with a short correlation time. The reported TGI sources include the intensity fluctuation of quasi-continuous multimode lasers [6], amplified spontaneous emission (ASE) light [25, 30], random fiber lasers [14, 31, 32], and pseudo-random coded light [7, 33, 34]. The laser intensity fluctuations and the ASE light have a small amplitude, which requires optical amplification. Random fiber lasers can generate a large-amplitude random waveform, but usually require a long fiber and a high-power pump light source, leading to complex configurations hard to integrate. The methods using pseudo-random coded light

* Corresponding author (email: abwang@gdut.edu.cn)

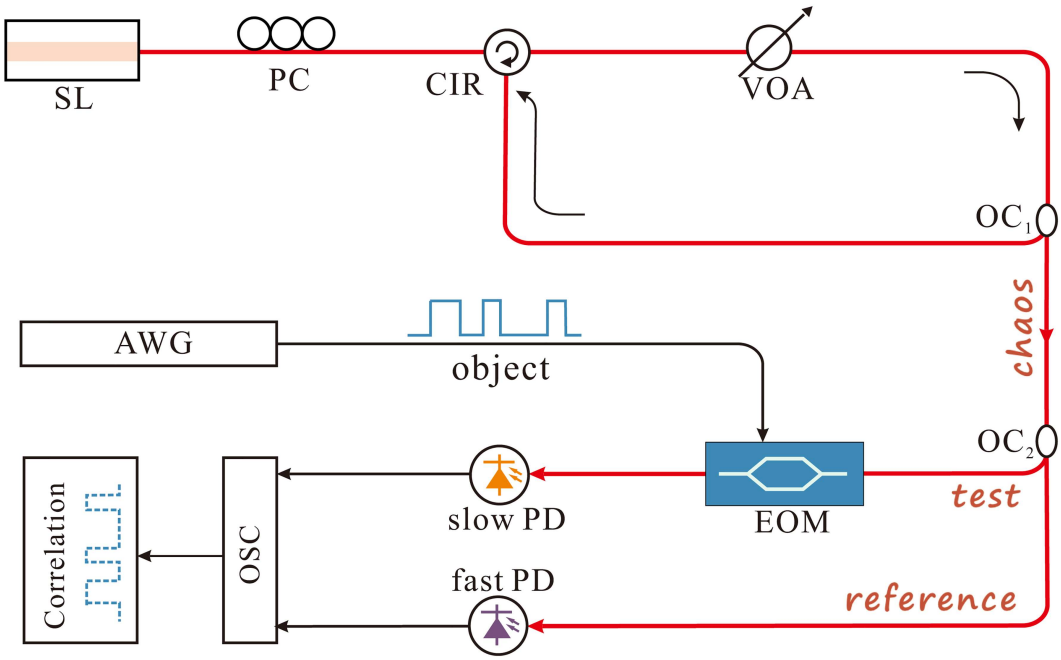

Figure 1 (Color online) Experimental setup of optical-chaos TGI. SL: semiconductor laser; PC: polarization controller; CIR: circulator; OC: optical coupler; VOA: variable optical attenuator; AWG: arbitrary waveform generator; EOM: electro-optic modulator; PD: photodetector; OSC: oscilloscope.

face the challenge of limited sequence length, which restricts the time size of imaging. In addition, the imaging of high-speed objects also requires expensive high-speed random code generation devices.

Optical chaos based on the nonlinearity of optoelectronic devices can be a promising alternative source for TGI, because it has large-amplitude and wideband random waveforms [35–41]. Especially, optical chaos can be generated by using semiconductor lasers with simple structures that are highly compatible with photonic integration [42–45]. Chen et al. [46] numerically demonstrated the feasibility of TGI using a chaotic laser. However, no experiments about optical-chaos TGI have been reported.

In this paper, we experimentally demonstrate the optical-chaos TGI by using an optical-feedback semiconductor laser. TGI for an 8-Gbit/s non-return-to-zero (NRZ) signal is achieved by using a laser with a relaxation frequency of about 6 GHz. Effects on TGI of chaos spectrum flatness and feedback time delay signature are investigated in detail. Experimental results show that chaotic laser is an effective light source for TGI with simple and low-cost configuration.

2 Experimental setup

Figure 1 shows the experimental setup of the proposed optical-chaos TGI. The optical chaos is generated by a semiconductor laser subject to external optical feedback. A portion of the laser emission is fed back through an optical coupler OC_1 and an optical circulator into the laser to induce chaos. A variable optical attenuator is inserted into the feedback path to adjust the feedback strength, which is denoted as κ_{f} and defined as the power ratio between the feedback light and the solitary laser. The generated chaotic light is divided into two beams, serving as reference and test light. The reference light is directly measured by a fast photodetector as a reference denoted as $I_{\mathrm{ref}}(t)$. The test beam is modulated by a temporal object $m(t)$ and then measured as a signal $I_{\mathrm{test}}(t)$ by a slow photodetector. The temporal waveforms of the two signals are recorded by a real-time oscilloscope, and then are used to reconstruct the object by cross-correlation calculation. The reconstructed object $m'(t)$ is calculated as

$$m'(t) = \langle \triangle I_{\mathrm{test}}(t) \triangle I_{\mathrm{ref}}(t) \rangle_M, \tag{1}$$

where $\triangle I_{\mathrm{ref}}(t)$ and $\triangle I_{\mathrm{test}}(t)$ are the reference and test signals after removing the mean value, respectively, and $\langle \cdot \rangle_M$ denotes the average of M repeated measurements.

In our experiments, the laser used is a distributed feedback (DFB) semiconductor laser with a single-longitudinal-mode at a wavelength of 1547.924 nm and a threshold current of 12.2 mA. The propagation time of light in the

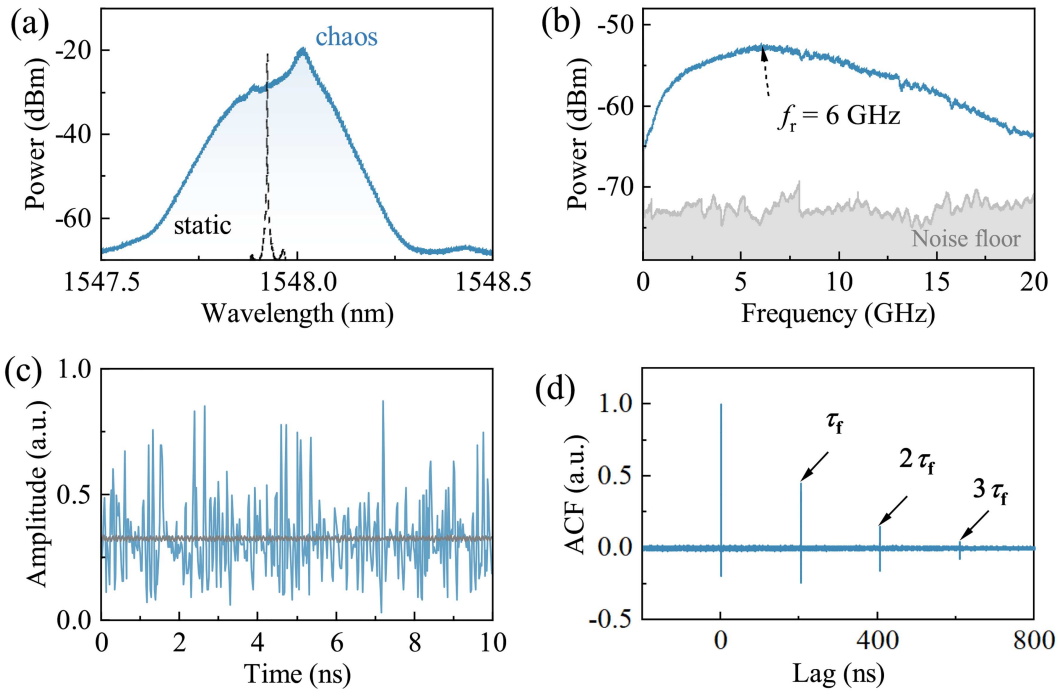

Figure 2 (Color online) Output characteristics of chaotic optical-feedback laser: (a) optical spectrum, (b) electrical spectrum, (c) single-measurement temporal waveform (blue) and averaged waveform (gray) with 6000 measurements, (d) autocorrelation trace. $\kappa_f = 17.73\%$, $\tau_f = 202.73$ ns.

feedback loop, i.e., feedback delay time τ_f, is 202.73 ns. The temporal object is generated by an arbitrary waveform generator (Keysight M8195A, 25-GHz bandwidth). An electro-optic modulator with 30-GHz bandwidth (iXblue MX-LN-40) is employed to load the temporal object onto the test light. The used fast and slow photodetectors have bandwidths of 52 GHz (Finisar XPDV2120RA) and 1 GHz, respectively. Note that the actual detection bandwidth of the reference signal is limited to 23 GHz by the used real-time oscilloscope (Tektronix DPO75902SX). In addition, we utilized an optical spectrum analyzer (APEX AP2060A) and an RF spectrum analyzer (R&S FSW50) to observe the frequency-domain characteristics of chaotic laser.

NRZ signals are used as the temporal object to experimentally demonstrate the chaos TGI. Quality factor $Q = (\langle m'_1\rangle - \langle m'_0\rangle)/(\sigma_1 + \sigma_0)$ is utilized to quantitatively evaluate the quality of the recovered temporal signals. Here, $\langle m'_i\rangle$ and σ_i are the mean value and standard deviation of high levels ($i = 1$) or low levels ($i = 0$) of NRZ signal $m'(t)$. The successful TGI is achieved as Q exceeds a threshold $Q_{\rm th} = 2.67$, which corresponds to the bit-error-rate threshold of 3.8×10^{-3} for the hard-decision forward error correction (HD-FEC).

3 Experimental results

3.1 Demonstration of optical-chaos TGI

Figure 2 shows the time-frequency characteristics of laser chaos, which were experimentally obtained with a laser bias current of 22.0 mA and feedback strength κ_f of 17.73%. As plotted in Figure 2(a), the optical spectrum of chaotic laser is obviously broadened and red shifted, compared to the static-laser spectrum. The corresponding electrical spectrum is broadband and extends over 20 GHz. Note that there is a peak at about 6 GHz, which is the laser relaxation oscillation frequency f_r. Shown in Figure 2(c), the temporal waveform of laser chaos is complex and irregular with a larger amplitude, and the average of 6000 waveforms remains constant. Furthermore, the chaotic waveform has a delta-like autocorrelation trace, shown in Figure 2(d). These characteristics indicate that laser chaos can satisfy the TGI requirement. It is noted that the autocorrelation trace has feedback time delay signature (TDS), which means a few small side-peaks located at $n\tau_f$, where $n = 1, 2, 3, \ldots$. The effects of TDS on the TGI quality will be discussed later.

Figures 3(a) and (b) show the experimental results of optical-chaos TGI for NRZ signals with a rate of 5 and 8 Gbit/s, respectively. The object length per measurement is 10 ns, and the total duration corresponding to $M = 6000$ is 6 μs. The NRZ signal amplitude applied to the EOM is 0.086 times the half-wave voltage $V_{\pi\rm RF}$. The first

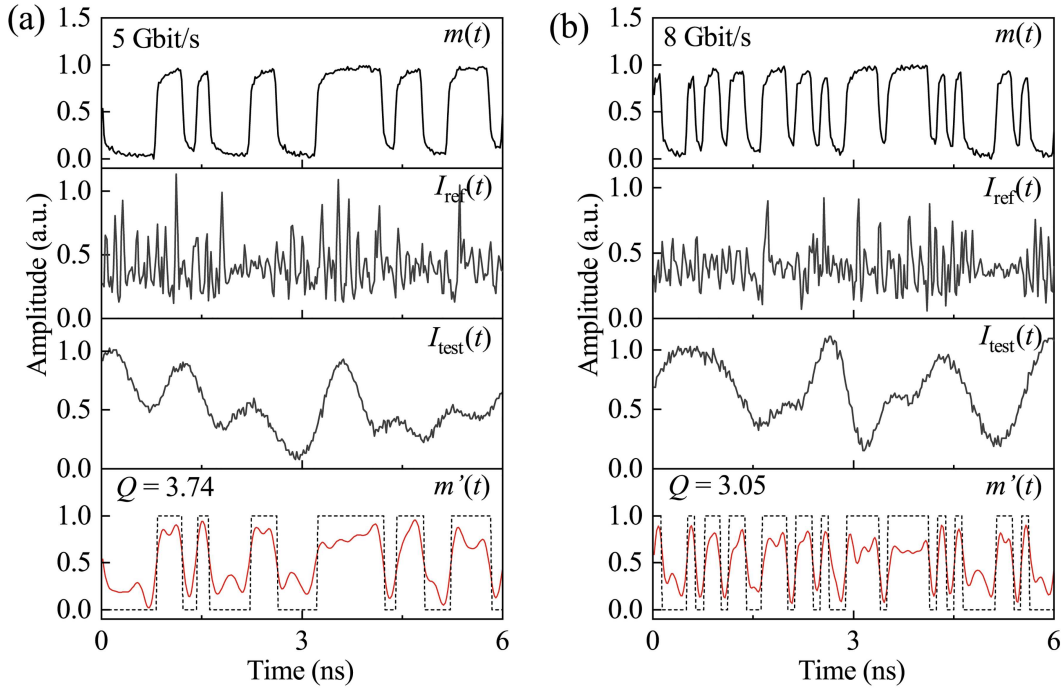

Figure 3 (Color online) Experimental results of optical-chaos TGI with $\kappa_f = 17.73\%$ and $M = 6000$ for NRZ signals at a rate of (a) 5 Gbit/s and (b) 8 Gbit/s.

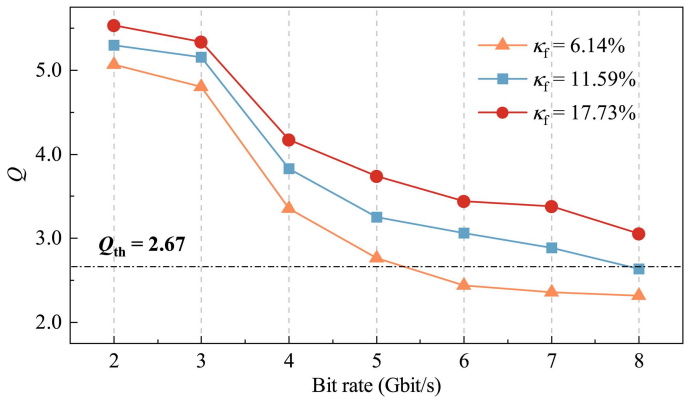

Figure 4 (Color online) Quality factor of object recovery at different bit rates. $M = 6000$.

to the third rows in Figure 3 show the temporal waveforms of the original object $m(t)$ directly emitted from the arbitrary waveform generator, the reference signal $I_{\mathrm{ref}}(t)$, and the test signal $I_{\mathrm{test}}(t)$, respectively. The test signal does not exhibit the characteristics of the object and the reference, due to the small-amplitude modulation and low-bandwidth detection. The fourth row in Figures 3(a) and (b) displays the recovered objects by the TGI. Bit "0" and "1" levels are clearly distinguished, and the waveforms are highly similar to the original signals. The TGI quality factors are 3.74 and 3.05 at signal rates of 5 and 8 Gbit/s, respectively, both of which exceed the threshold Q_{th}. Therefore, the laser-chaos TGI is successfully achieved. Additionally, the bandwidth of slow PD required for TGI can be narrower. A slow PD bandwidth exceeding 300 MHz is needed for 5 Gbit/s, while exceeding 400 MHz is required for 8 Gbit/s. It also enables reconstruction at a weaker modulation depth, with the 5 Gbit/s object successfully reconstructed at 0.028 $V_{\pi\mathrm{RF}}$. If a multi-level signal is used as the object, a higher modulation depth is required to ensure the distinguishability of each level in the reconstruction.

Figure 4 displays the TGI quality factor as a function of the signal bit rate, which was obtained under the same object modulation amplitude. The results of different feedback strengths $\kappa_f = 6.14\%$, 11.59% and 17.73% consistently show that the quality factor gradually decreases as the signal rate increases. The reason is that the energy of the object signal within the slow PD bandwidth decreases as its rate increases, resulting in a decrease in signal-to-noise ratio. In addition, the results indicate that a high feedback strength will result in a larger quality

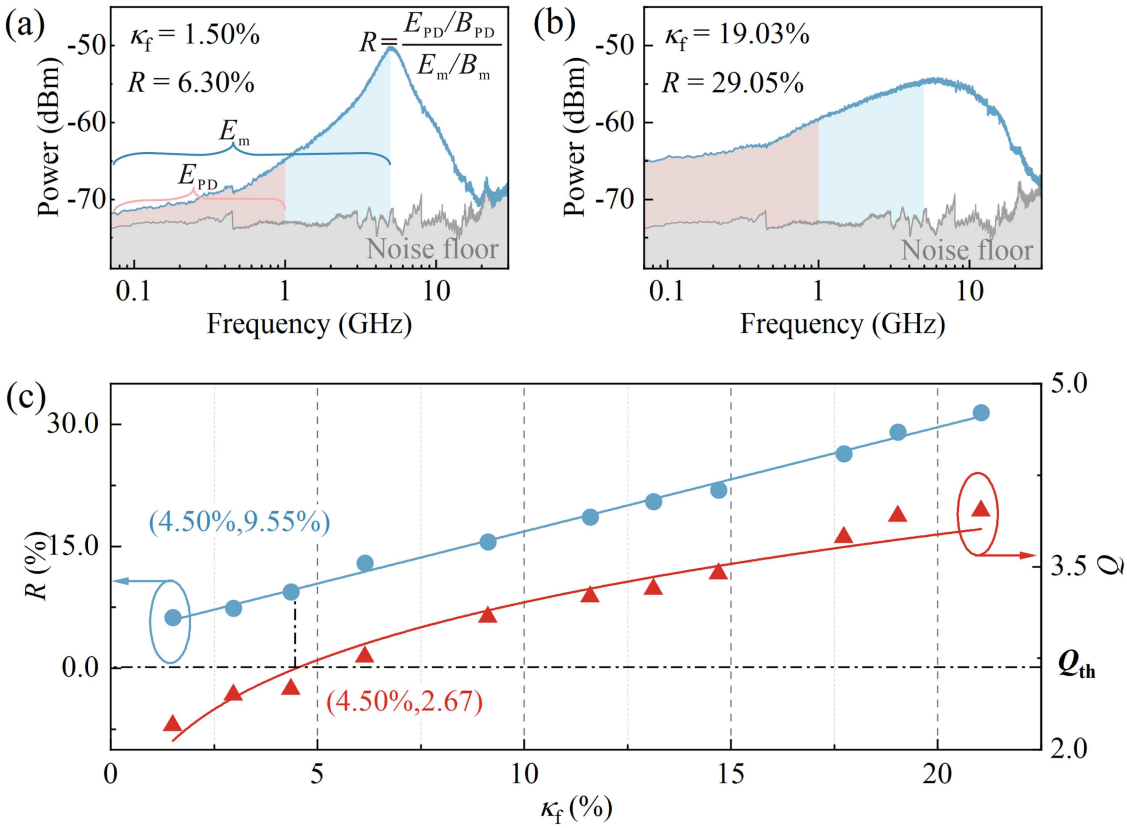

Figure 5 (Color online) Effect of laser feedback strength on optical-chaos TGI with the object rate of 5 Gbit/s. (a), (b) Electrical spectra of laser chaos under $\kappa_f = 1.50\%$ and 19.03%, where E_{PD}, E_m are the energy within the slow PD bandwidth and the energy within the signal baseband, and $R = (E_{PD}/B_{PD})/(E_m/B_m)$; (c) R (solid circles) and Q (triangles) vs. κ_f.

factor. This can be attributed to the fact that the low-frequency component of laser chaos becomes strong as feedback strength increases.

3.2 Effects of laser feedback strength

In this subsection, we investigate the effects of laser feedback strength κ_f on TGI quality in detail. Figures 5(a) and (b) plot the electrical spectra of chaotic laser under $\kappa_f = 1.50\%$ and 19.03%, respectively. In the case of large feedback, the spectrum is wider and flatter. Especially, the low-frequency components within the bandwidth of slow PD become stronger, depicted in the red shaded area. This is beneficial for improving the signal-to-noise ratio of TGI. For quantitative analysis, we define $R = (E_{PD}/B_{PD})/(E_m/B_m)$ to evaluate the spectrum flatness, where E_{PD}, E_m are the energy within the slow PD bandwidth B_{PD} and the energy within the signal baseband width B_m. Figure 5(c) shows R and Q as functions of κ_f in solid circles and triangles. As the feedback strength increases, R grows almost linearly, and the TGI quality factor increases at a gradually decreasing rate. When $\kappa_f > 4.50\%$, $R > 9.55\%$, and the quality factor of the reconstructed object exceeds the threshold 2.67, meaning a successful TGI. A higher Q value close to 4 can be achieved with $R > 30.00\%$. The above results indicate that chaotic lasers can enable a high-quality TGI, although their spectra are not as flat as noise signals.

3.3 Effects of time delay signature

It is noted that increasing the feedback strength not only improves the spectrum flatness, but also enhances the feedback time delay signature [47]. In other words, the effect of the laser feedback strength on TGI actually includes the contribution of TDS. Therefore, it is also interesting to understand how the feedback time delay signature alone affects the imaging results.

The level of TDS is measured by the first sidelobe peak of the autocorrelation function (ACF) of the laser chaos. It is hard to change TDS while keeping spectral flatness R fixed by adjusting the operating parameters of the optical-feedback laser. In experiments, we adopted a data reconstruction method to solve this problem. The sampled laser chaos is denoted as a discrete sequence $X = (x_0, x_1, \ldots, x_{N-1})$, and then the TDS is $\mathrm{ACF}_X(N_f)$, where N_f is the

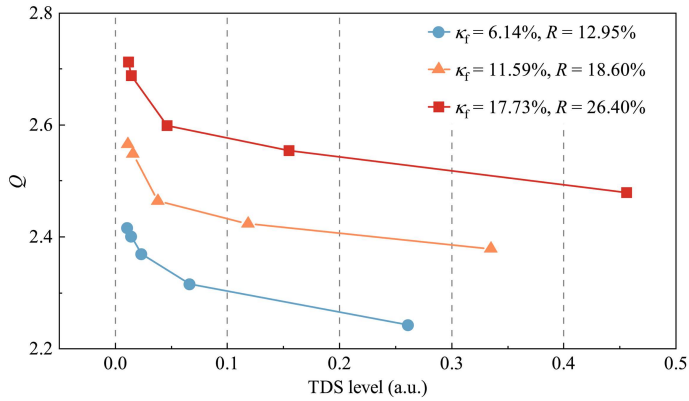

Figure 6 (Color online) Effect of TDS on optical-chaos TGI with the rate of 5 Gbit/s and $M = 1990$.

datapoint index corresponding to τ_f. One extracts N_f-point sub-sequences $Xs_k = (x_{kjN_f}, x_{kjN_f+1}, \ldots, x_{kjN_f+N_f-1})$ from X with an interval of $(j-1)N_f$ points, where $k = 0, 1, 2, \ldots$, and then generate a new sequence $Y = \{Xs_0, Xs_1, Xs_2, \ldots\}$. Then, the TDS of sequence Y is $\mathrm{ACF}_Y(N_f) = \mathrm{ACF}_X(jN_f)$, where j is a positive integer. Due to that the ACF of the original chaos has different sidepeak values shown in Figure 2(d), one can change integer j to obtain different $\mathrm{ACF}_Y(N_f)$ without influence on chaos spectrum.

Figure 6 plots the effects of the TDS on the TGI quality factor, which were experimentally obtained with different feedback strengths of 6.14%, 11.59%, and 17.73%. The results under the three cases agree well that the Q decreases with the growth of TDS. Fortunately, the rate of decrease gradually slows down, and the magnitude of the decrease is relatively small, which is about 0.2. According to Figures 5 and 6, we can conclude that the time delay signature of laser chaos will slightly reduce the Q value but will not lead to failure of TGI. The dominant factor affecting the Q value is the spectral flatness or low-frequency energy of laser chaos. Here, the length of the data stored by the oscilloscope is 10 μs. After discarding irrelevant data, the maximum of M is 1990 for evaluating TGI results with different j values in Figure 6. However, this does not affect the conclusion about the effects of TDS on the TGI quality factor.

4 Discussion and conclusion

The optical-chaos TGI is achieved, although the chaotic light has a non-flat spectrum and feedback time delay signature. To further improve the TGI quality and rate, optimization can focus on spectral flattening, TDS suppression, chaotic bandwidth expansion, and object modulation. Based on the recent broadband chaos study of long-cavity FP laser, the object reconstruction rate can be expected to reach 16 Gbit/s [48]. To reduce the measurement times, multiplexing techniques can be considered [7]. In addition, the chaotic laser used is composed of discrete components connected by optical fiber. Photonic integration of chaotic lasers can significantly improve the robustness [42–45, 49]. Considering the successful implementation of chaos in other bands such as THz, TGI shows broad application potential [50]. Furthermore, laser chaos has a unique characteristic of chaos synchronization compared to other TGI sources [42, 49, 51, 52]. Combining chaos synchronization, it is expected to develop a new paradigm for information encryption transmission.

In conclusion, we experimentally demonstrate optical-chaos TGI using an external optical-feedback semiconductor laser. Effects of feedback strength and time delay signature are investigated. Results show that the low-frequency energy of the chaos spectrum within the bandwidth of the slow detector is the dominant factor affecting the imaging quality. TGI with a quality factor beyond 3 for 8-Gbit/s NRZ signals is achieved by using a chaotic laser with a relaxation frequency of 6 GHz and 1-GHz detection bandwidth. In the future, we will study the photonic integration of chaotic lasers to improve imaging performance and explore TGI-based secure information transmission by combining chaos synchronization.

Acknowledgements This work was supported by National Natural Science Foundation of China (Grant Nos. 62035009, U22A2087), Guangdong Introducing Innovative and Entrepreneurial Teams of "the Pearl River Talent Recruitment Program" (Grant No. 2019ZT08X340), and Natural Science Foundation of Shanxi Province (Grant No. 202403021211159).

References

1 Pittman T B, Shih Y H, Strekalov D V, et al. Optical imaging by means of two-photon quantum entanglement. Phys Rev A, 1995, 52: R3429–R3432
2 Sephton B, Nape I, Moodley C, et al. Revealing the embedded phase in single-pixel quantum ghost imaging. Optica, 2023, 10: 286–291

3 Bennink R S, Bentley S J, Boyd R W. "Two-Photon" Coincidence imaging with a classical source. Phys Rev Lett, 2002, 89: 113601
4 Chen Y F, Tian T, Lu X, et al. Attention-enhanced computational ghost imaging. Sci China Inf Sci, 2025, 68: 162104
5 Kolner B H. Space-time duality and the theory of temporal imaging. IEEE J Quantum Electron, 1994, 30: 1951–1963
6 Ryczkowski P, Barbier M, Friberg A T, et al. Ghost imaging in the time domain. Nat Photon, 2016, 10: 167–170
7 Devaux F, Moreau P A, Denis S, et al. Computational temporal ghost imaging. Optica, 2016, 3: 698–701
8 Shirai T, Setälä T, Friberg A T. Temporal ghost imaging with classical non-stationary pulsed light. J Opt Soc Am B, 2010, 27: 2549–2555
9 Faccio D. Temporal ghost imaging. Nat Photon, 2016, 10: 150–152
10 Huang X, Bai Y, Fu X. Stable and secure image transmission based on temporal ghost imaging. J Opt, 2019, 21: 055701
11 Wang Y, Chen H, Jiang W, et al. Optical encryption for visible light communication based on temporal ghost imaging with a micro-LED. Opt Lasers Eng, 2020, 134: 106290
12 Ryczkowski P, Barbier M, Friberg A T, et al. Magnified time-domain ghost imaging. APL Photonics, 2017, 2: 046102
13 O-oka Y, Fukatsu S. Differential ghost imaging in time domain. Appl Phys Lett, 2017, 111, 061106
14 Wu H, Ryczkowski P, Friberg A T, et al. Temporal ghost imaging using wavelength conversion and two-color detection. Optica, 2019, 6: 902–906
15 Kang Y, Zhang L, Ye H, et al. One-to-many optical information encryption transmission method based on temporal ghost imaging and code division multiple access. Photon Res, 2019, 7: 1370–1380
16 Chen X, Jin M, Chen H, et al. Computational temporal ghost imaging for long-distance underwater wireless optical communication. Opt Lett, 2021, 46: 1938–1941
17 Wang Y, Jiang W, Chen H, et al. Ultra-high frequency signal transmission based on temporal ghost imaging. J Lightwave Technol, 2022, 40: 5426–5431
18 Wu H, Hu B, Chen L, et al. Mid-infrared computational temporal ghost imaging. Light Sci Appl, 2024, 13: 124
19 Zhao J, Tang Z, Shao K, et al. Full-duplex optical communication system based on computational temporal ghost imaging. J Lightwave Technol, 2024, 42: 8229–8236
20 He L, Hu B, Bo Z, et al. Mid-infrared data encryption and transmission beyond detector bandwidth based on frequency down-conversion temporal ghost imaging. APL Photonics, 2025, 10: 056104
21 Yao X, Zhang W, Li H, et al. Long-distance thermal temporal ghost imaging over optical fibers. Opt Lett, 2018, 43: 759–762
22 Zhou D P, Peng W, Chen L, et al. Computational distributed fiber-optic sensing. Opt Express, 2019, 27: 17069–17079
23 Zhao J, Dai J, Braverman B, et al. Compressive ultrafast pulse measurement via time-domain single-pixel imaging. Optica, 2021, 8: 1176–1185
24 Wang F X, Wu J, Chen W, et al. Perceiving quantum hacking for quantum key distribution using temporal ghost imaging. Phys Rev Appl, 2021, 15: 034051
25 Wu J, Wang F X, Chen W, et al. Temporal ghost imaging for quantum device evaluation. Opt Lett, 2019, 44: 2522–5225
26 Zhang L, Liu F, Zhong H, et al. Performance evaluation of plastic optical fiber communication using micro-lens coupling and computational temporal ghost imaging algorithm. Opt Express, 2023, 31: 18993–19005
27 Ratner D, Cryan J P, Lane T J, et al. Pump-probe ghost imaging with SASE FELs. Phys Rev X, 2019, 9: 011045
28 Imani M F, Smith D R. Temporal microwave ghost imaging using a reconfigurable disordered cavity. Appl Phys Lett, 2020, 116: 054102
29 O-oka Y, Keyaki R, Fujisawa S, et al. One-time readout temporal single-pixel imaging. Opt Lett, 2023, 48: 3307–3310
30 Tang J, Tang Y W, He K, et al. Computational temporal ghost imaging using intensity-only detection over a single optical fiber. IEEE Photonics J, 2018, 10: 7101809
31 Wu H, Han B, Wang Z, et al. Temporal ghost imaging with random fiber lasers. Opt Express, 2020, 28: 9957–9964
32 Ni L Q, Qi Y F, Bao X Y, et al. Temporal-spectral correlation dynamics of Raman random fiber laser. Sci China Inf Sci, 2025, 68: 140404
33 Xu Y K, Sun S H, Liu W T, et al. Detecting fast signals beyond bandwidth of detectors based on computational temporal ghost imaging. Opt Express, 2018, 26: 99–107
34 Kang Y, Zhang L H, Zhang D W. Study of an encryption system based on compressive temporal ghost imaging with a chaotic laser. Opt Commun, 2018, 426: 535–540
35 Argyris A, Syvridis D, Larger L, et al. Chaos-based communications at high bit rates using commercial fibre-optic links. Nature, 2005, 438: 343–346
36 Uchida A, Amano K, Inoue M, et al. Fast physical random bit generation with chaotic semiconductor lasers. Nat Photon, 2008, 2: 728–732
37 Sciamanna M, Shore K A. Physics and applications of laser diode chaos. Nat Photon, 2015, 9: 151–162
38 Didier P, Zaminga S, Spitz O, et al. Data encryption with chaotic light in the long wavelength infrared atmospheric window. Optica, 2024, 11: 626–633
39 Wang A B, Wang Y C. Chaos correlation optical time domain reflectometry. Sci China Inf Sci, 2010, 53: 398–404
40 Yamazaki T, Uchida A. Performance of random number generators using noise-based superluminescent diode and chaos-based semiconductor lasers. IEEE J Sel Top Quantum Electron, 2013, 19, 0600309
41 Xiong H H, Jiang N, Li A R, et al. Chaotic optoelectronic oscillators-based dual-function radar-communication system. Sci China Inf Sci, 2025, 68: 192302
42 Argyris A, Hamacher M, Chlouverakis K E, et al. Photonic integrated device for chaos applications in communications. Phys Rev Lett, 2008, 100: 194101
43 Wu J G, Zhao L J, Wu Z M, et al. Direct generation of broadband chaos by a monolithic integrated semiconductor laser chip. Opt Express, 2013, 21, 23358–23364
44 Chai M M, Qiao L J, Li S H, et al. Wavelength-tunable monolithically integrated chaotic semiconductor laser. J Lightw Technol, 2023, 41: 5952–5957
45 Hu S, Wang Q, Zhang F, et al. Nonlinear dynamics of hybrid integrated laser based on self-seeding of a DFB-LD by using a Si_3N_4 microring resonator as filter feedback. Chaos Solitons Fractals, 2025, 190: 115776
46 Chen Z, Li H, Li Y, et al. Temporal ghost imaging with a chaotic laser. Opt Eng, 2013, 52: 076103
47 Rontani D, Locquet A, Sciamanna M, et al. Loss of time-delay signature in the chaotic output of a semiconductor laser with optical feedback. Opt Lett, 2007, 32: 2960–2962
48 Li Q, Jia Z, Wang A, et al. Parallel generation of multi-channel broadband chaos by a long-cavity FP laser with optical feedback. Opt Lett, 2024, 49: 7126–7129
49 Sasaki T, Kakesu I, Mitsui Y, et al. Common-signal-induced synchronization in photonic integrated circuits and its application to secure key distribution. Opt Express, 2017, 25: 26029–26044
50 Liu B, Silvestri C, Zhou K, et al. Terahertz semiconductor laser chaos. Nat Commun, 2025, 16: 9985
51 Wang L, Wang J, Wu Y, et al. Chaos synchronization of semiconductor lasers over 1040-km fiber relay transmission with hybrid amplification. Photon Res, 2023, 11: 953–960
52 Wang A, Du Y, Li Q, et al. Physical-layer key distribution using synchronous complex dynamics of DBR semiconductor lasers. APL Photonics, 2024, 9: 036109